中國機械工程學刊第四十卷第三期第 287~298 頁(民國一百零八年)
Journal of the Chinese Society of Mechanical Engineers, Vol.40, No.3, pp 287~298 (2019)

Gas Liquid Solid Three Phase Flow Separation Efficiency Simulation and Application in Design of Enclosed Sand Separator

Liangliang Dong*and Xiaohua Zhu**

Key words: gas liquid solid three phase flow, gas drilling enclosed sand; separator; sand removal efficiency; erosion; structural optimization

ABSTRACT

Because of high content of the gas powder dust (more than 1000 times the standard value), high flow rate and rapid gas flow, the gas drilling technique leads to serious pollution on the surrounding environment; besides, with respect to wells with H_2S, its application popularization is seriously curbed because the effective enclosed sulfur removal is not possible. In response to problems abovementioned, one type of gas liquid solid three phase flow two-stage Enclosed Sand Separator for gas drilling is put forward herein. At present, the numerical simulation for the gas liquid solid three phase flow separation is mainly intended for the two phase flow separation, and it’s possible to simulate three phase flow separation. The author uses the quasi three phase flow mode, splits the gas liquid solid three phase flow into gas liquid and gas solid two phase flow, and establishes the Euler multiphase flow numerical calculation model. Besides, the correctness of the simulated calculation result is verified based on experiments.When the flow field motion rule of gas, water and sand inside the separation device and sand separation efficiency are drawn through calculation by using such a model, the better system scheme is thus determined, and successfully applied in YangJia 1st well. Studies herein has provided the numerical simulation method for the calculation of the gas liquid solid three phase flow separation efficiency, and is of great significance to the application popularization of the gas drilling technique, enabling recycling gas drilling and improvement on the well pad operation environment.

INTRODUCTION

With the gradual improvement on the gas drilling technique, the gas drilling has realized rapid development thanks to its advantages as good efficiency, low cost and protection on the reservoir [1]. However, when the drill bit encounters H_2S, or in case the oil and gas intrudes, it shall be immediately switched to the slurry drilling, which significantly increases the occupancy rate of the field equipment; due to such characteristics as high content of crushed debris (sand), high flow rate, rapid gas flow, big span of the particle size of the powder dust, gas discharged from the gas drilling leads to the content of powder dust exceeding thousands of times the standard value, posing serious pollutions on the operation environment and environment surrounding the well pad. Especially in recent years, the urban hazy weather forces the environmental protection authority to shutdown projects with serious environmental pollution, which greatly curbs the application popularization of the gas drilling technique. In the meantime, when the cyclic media is nitrogen or natural gas, the direct discharge of the gas significantly increases the drilling cost. The recycling gas drilling technique is one of main means to resolve problems abovementioned. Besides, to separate sand from the gas flow has emerged as a crucial link of the recycling gas drilling technique.

Paper Received June, 2017. Revised January, 2018. Accepted January, 2018. Author for Correspondence: Xiaohua Zhu

* *Lecturer, School of Mechatronic Engineering, Southwest Petroleum University, Chengdu 610500, China*

** *Professor, School of Mechatronic Engineering, Southwest Petroleum University, Chengdu 610500, China*

The traditional gas solid separation devices, e.g. cyclone separator, bag dust catcher cannot meet with field needs due to such characteristics as the small dust processing capacity and easy consumption; the high voltage electrostatic dust removal method is greatly restricted by the operation condition of the well pad. At present, the gas drilling well pad mainly collects dust via the foundation pit, namely the exhaust from the gas drilling will be used to impact the preset foundation pit via the sand drainage pipeline so that the exhaust gradually spreads out in the foundation pit to reduce environmental pollution. This method is not efficient to remove dust. Besides, it's not effective to improve the well pad environment (as shown in Fig.1), and difficult to realize the gas recycling. With respect to the well containing H_2S, the gas produced from the gas drilling shall undergo enclosed sulfur and sand removal operation before meeting with the environmental protection requirements. Veteran Energy and Weatherford have developed the recycling gas technology [2-4]. However, abovementioned techniques don't give specific requirements on the sand removal so that plentiful sandy gas again enters the gas compressor and well hole, which leads to such problems as life compromise of the air compressor, difficulty of carrying rocks by the gas inside the well hole, and big content of sand in the environment air. Therefore, one type of Enclosed Sand Separator for gas drilling is urgently needed to effectively remove sand and H_2S arising out of the gas drilling. The authority has put forward one type of sand separator suitable for the gas drilling by comprehensively utilizing such methods as gravity, inertia and water bath separation.

Fig.1 Separate sands by foundation trench (left), and the pollution (right).

Traditional separation equipment is designed based on the empirical parameter. During operation, it may easily cause such problems [5-9] as vortex flow, return flow and uneven distribution of internal pressure field and velocity field, which usually leads to relatively low separation efficiency and unreasonable increment of the operation resistance [10]. The multiphase flow-based numerical simulation method is one of the main means to resolve abovementioned problems.

For the past decades, there're lots of work on simulation the flow field of separators. Some reports researched the flow field by using single phase flow, such as: Atakan Avci et al.[10] devoted to a new method for evaluating vortex length in reversed flow cyclone separators with single phase flow. Chuan Tian and Yijia Lu[11] set up the turbulence models of separated flow in shock wave thrust vector nozzle, and validated that k-epsilon gives the best results.

Two-phase flow simulation was studied to accurately simulate the flow field of separators. Shanhong Li et al. [12] simulated the motion rule of flow field inside the umbrella plate scrubber by using the Reynolds stress model to simulate gas phase, and discrete phase model to simulate the solid particle trajectory. W. Tanthapanichakoon et al. [13] studied the filtration performance of high-temperature exhaust in twin ceramic candles by using RNG model. K.W. Chu et al. [14] simulated the gas solid two phase flow inside the cyclone separator based on the discrete element model and computational fluid dynamics (CFD) model. M.S. Manju et al. [15] simulated the flow field of coal ash in the rotary kiln by taking the gas phase on the continuous phase, and putting in the continuous phase the solid phase as the Lagrangian coordinates. Rodrigo J.G. et al. [16] simulated the distribution rule of the flow field of the trickle bed based on Euler-Euler two phase flow model. Luca Marocco et al. [17] applied Euler -Lagrange multiphase flow model to the simulation of the wet desulphurization, and conducted experiments to verify accuracy of computation results. Xiana Romaní Fernández et al. [18] simulated the gas solid two phase flow inside the solid bowl centrifugal by using VOF model.

Sujeet Kumar Shukla et al.[19] simulated the effect of modeling of velocity fluctuations on prediction of collection efficiency of cyclone separators by using a gas-solid two phase model.

To get the separation efficiency conveniently, some researchers studied the separation efficiency compute method by simulation. Chang H. Jung and Yong P. Kim[20] computed the separation efficiency of aerosol separator. Morteza Eslamian[21] simulated the field flow of novel thermophoretic particle separators by setting the particle as a discrete phase.

Experiment method had been performed to calculate the separation efficiency. Xiang Gao et al.[22] studied the oil droplets separation performance and separation efficiency numerically and experimentally. Rainier Hreiz et al.[23] experimentally studied the effect of the nozzle design on the performances of gas-liquid cylindrical cyclone separators. Zhiyi Xiong et al.[24] experimentally researched the development of a gas-solid cyclone separator with high efficiency and low pressure drop in axial inlet cyclones. Zhenqin Xiong et al.[25] studied on flow pattern and separation performance of air-water swirl-vane separator with Euler two-phase model and RSM turbulence model and validated experimentally. Irfan Karagoz et al.[26] designed and performance evaluated of a new cyclone separator.

However, there’s only Benjamin Kaku Arvoh et al.[27] estimated of gas/liquid and oil/water interface levels in an oil/water/gas separator. And this paper introduced an experimental method to calculate interface levels. However, report on the study of gas liquid solid three phase separation remains rare. The author uses the quasi three phase flow mode, splits the gas liquid solid three phase flow into gas liquid and gas solid two phase flow, and establishes the gas liquid solid three phase flow field simulation model; the flow field motion rule and sand removal efficiency have been calculated. By taking the Enclosed Sand Separator designed as an example, the simulation model established will be used for structural optimization, and it has been successfully utilized in the field.

STRUCTURE AND PRINCIPLE

Brief structure of the Enclosed Sand Separator for gas drilling is given in Fig.2; the separation device designed is mainly composed of three phase mixer, one stage separation tank, sand removal baffle, two stage separation tank, sand drainage pump, submerged sieve pipe, dedusting liquid, etc.

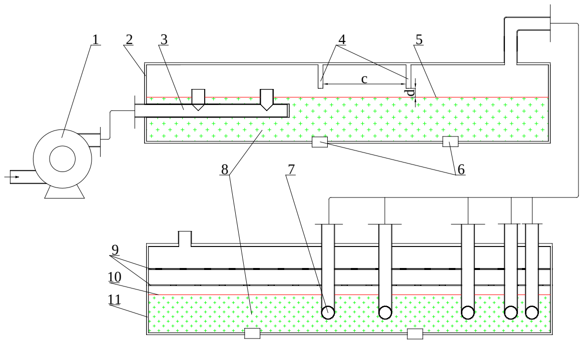

Fig. 2 Brief structure of Enclosed Sand Separator

1 three phase separator, 2 one-stage separation tank, 3 inlet pipeline, 4 sand removal baffle (one stage separation tank), 5 dedusting liquid surface (one stage separation tank), 6 sand drainage pump, 7 submerged seive pipe, 8 dedusting liquid, 9 sand removal baffle (two-stage separation tank), 10 dedusting liquid surface (two stage separation tank), 11 two stage separation tank.

Mixed phase of gas and sand discharged during gas drilling firstly undergo three phase mixer; the gas liquid solid three phase flow is formed when the gas sand is again mixed a certain amount of water. Via the inlet pipeline, it enters the one-stage separation tank; the gas liquid solid three phase flow after separation will pass through outlet of one stage separation tank and external connection pipeline, and flow into the dedusting liquid of the two-stage separation tank via the submerged sieve pipe; after separation by the two stage separation tank, the gas flow will be recycled or directly vented to the atmosphere via the outlet. During the drilling operation with H_2S, the separation tank will be added with the desulphurizing reagent to remove H_2S within the gas flow. In order to improve the dedusting efficiency of the sand separator designed, the one stage separation tank is equipped with two baffles; the bottom of the two-stage separation tank has reserved a certain amount of dedusting liquid; the bottom of the device is designed with the sand drainage pump so that the sand in the dedusting liquid can be timely discharged. The one stage separation tank can remove solid particle with a size of more than 100μm while the two stage separation is mainly intended for the powder dust with a size of more than 1μm.

NUMERICAL MODEL

Gas phase control equation

Among the gas, liquid and solid three phase flow, the gas phase accounts for as much as 99.71% with respect to the volume fraction. Therefore, the gas phase is defined as the continuous phase, and its control equation adopts the standard k-ε model. The transport equation corresponding to the gas phase [28]:

$$\frac{\partial}{\partial t}(\rho k)+\frac{\partial}{\partial x_i}(\rho k u_i)=\frac{\partial}{\partial x_j}\left[\left(\mu+\frac{\mu_t}{\sigma_k}\right)\frac{\partial k}{\partial x_j}\right]+G_k+G_b-\rho\varepsilon-Y_M+S_k \tag{1}$$

$$\frac{\partial}{\partial t}(\rho\varepsilon)+\frac{\partial}{\partial x_i}(\rho\varepsilon u_i)=\frac{\partial}{\partial x_j}\left[\left(\mu+\frac{\mu_t}{\sigma_\varepsilon}\right)\frac{\partial \varepsilon}{\partial x_j}\right]+C_{1\varepsilon}\frac{\varepsilon}{k}\left(G_k+C_{3\varepsilon}G_b\right)-C_{2\varepsilon}\rho\frac{\varepsilon^2}{k}+S_\varepsilon \tag{2}$$

Where: ρ media concentration; k turbulence energy; u_i fluid velocity in i direction; $C_{1\varepsilon}$, $C_{2\varepsilon}$ and $C_{3\varepsilon}$ empirical constant, σ_k and σ_ε Prandtl number respectively corresponding to turbulence energy k and dissipation rate ε. Dissipation rate of turbulence energy ε is defined as:

$$\varepsilon=\frac{\mu}{\rho}\overline{\left(\frac{\partial u_i'}{\partial x_k}\right)\left(\frac{\partial u_i'}{\partial x_k}\right)} \tag{3}$$

Turbulence viscosity may be expressed as:

$$\mu_t=\rho C_\mu\frac{k^2}{\varepsilon} \tag{4}$$

Production item of turbulence energy k arising out of the average velocity gradient:

$$G_k=\mu_t\left(\frac{\partial u_i}{\partial x_j}+\frac{\partial u_j}{\partial x_i}\right)\frac{\partial u_i}{\partial x_j} \tag{5}$$

Because the gas is the compressible fluid, the production item of the turbulence energy arising out of buoyance:

$$G_b=\alpha g_i\frac{\mu_t}{\Pr_t}\frac{\partial T}{\partial x_i} \tag{6}$$

Where: $\Pr_t$ Prandtl number of turbulence energy, g_i component of acceleration of gravity in i direction, α coefficient of thermal expansion, and it may be expressed as:

$$\alpha=-\frac{1}{\rho}\frac{\partial\rho}{\partial T} \tag{7}$$

Y_M contribution of pulse expansion to the compressible turbulence; for the compressible fluid:

$$Y_M=2\rho\varepsilon M_t^2 \tag{8}$$

Where: $M_t=\sqrt{k/a^2}$, a acoustic velocity.

Liquid, solid phase control equations

With respect to the gas fluid solid three phase flow of the dedusting equipment, because water and sand totally accounts for 0.29% of the volume fraction, water and sand may be deemed as the second phase; the quasi three phase flow Euler multiphase flow model is used for simulation; the three-phase flow formed by gas, water and sand is simplified as the two-type two phase flow of gas liquid and gas solid mixed by the gas and water, and gas and sand. Thus, the fluid model is called the model for three phase flows. When such scenarios as heat transfer and reaction are not taken into account, the mass balance equation (continuity equation) and momentum balance equation of quasi three phase flow model are given in equation 9 and 10 [26]:

$$\frac{\partial}{\partial t}\left(\varphi_p\rho_p\right)+\nabla\left(\varphi_p\rho_p\overline{\mu_p}\right)=0 \tag{9}$$

$$\frac{\partial}{\partial t}\left(\varphi_p\rho_p\overline{\mu_p}\right)+\nabla\left(\varphi_p\rho_p\overline{\mu_p\mu_p}\right)=-\varphi_p\nabla P_g+\nabla\left(\overline{\overline{E_p}}-\overline{\overline{E_1^f}}\right)+\overline{F_p}+\varphi_p\rho_p\overline{g} \tag{10}$$

Where: subscript p phase, $p=g$ gas phase, $p=l$ liquid phase, $p=s$ solid phase, φ phase volume fraction, superscript f pulse momentum, F_p interphase force, E_p viscous stress.

In the equation above, two items on left respectively mean time and convection; those on right respectively static pressure, expansion, drag and graviton between gas solid or gas liquid. The drag force between gas solid phase may be expressed as:

$$\overline{F_p}=\beta\left(u_{s,p}-u_{g,p}\right) \tag{11}$$

Where, β function of drag force between two phases, and it can be expressed as:

$$\beta = \frac{3}{4} C_D \frac{\varphi_s \varphi_g \rho_g \left| \overline{v_g} - \overline{v_s} \right|}{d_s} f\left(\varphi_g\right) \tag{12}$$

Similarly, the expression formula of drag force between gas and liquid phase can be drawn.

Model establishment

The finite element model for flow field computing for the sand separator is established by using the gas liquid solid three phase control equation mentioned in section 3.1 and 3.2. In order to increase the quantity of elements for the flow field model of each tank body, and further improve computing accuracy and efficiency, two separation tanks of the sand separator are respectively calculated, and the circulation pump at the bottom of the tank is simplified as the outlet. Because structure inside the tank is complex, the classification is made by the tetrahedron element.

In order to make the equipment better meet with the gas drilling needs, three phase flow rates in the inlet of the one-stage separation tank are all calculated as per the maximum value, with inlet gas flow 200m^3/min, liquid flow 0.5m^3/min, and solid flow 178kg/min; besides, the phase flow in the outlet of the one-stage separation tank will be taken as the flow in the inlet of the two-stage separation tank. Because diameters of particles contained in the gas discharged mostly center in between 0.01-0.5mm, it's assumed that the liquid and solid phases in the inlet of the two-stage separation tank are evenly distributed, with diameter of solid particle in the inlet of the one-stage separation tank 0.1mm, and diameter of particle in the inlet of the two-stage separation tank 0.01mm. The pressure outlet will be used, with the pressure at the standard atmospheric pressure. The calculation of the wall surface is subject to the escape discrete phase boundary condition, and the change of momentum is produced due to the rebound of particle here.

Model validation

In order to validate correctness of the simulation calculation results, experiment conditions in literature [29] has been analyzed. Because the experience conditions represent the separation of the gas solid two phase, the volume fraction of liquid phase is taken as 0 during the model validation. Because the separation of liquid phase in the Enclosed Sand Separator designed doesn't pose influence on the sand separation effect, and the existence of liquid phase will not cause safety incident, the separation effect of gas solid phase may be used to validate the correctness of computation method. Contrast of simulation computation results and experiment results is given in Fig. 3.

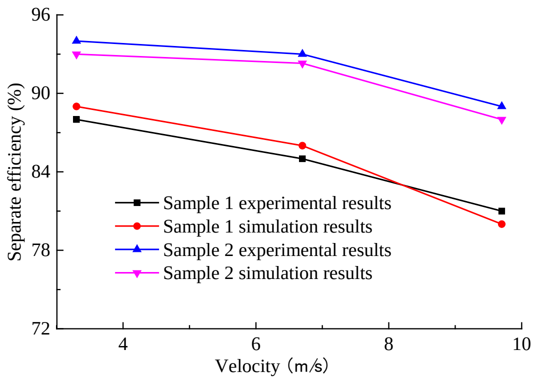

Fig. 3 Compare of the experimental results and simulation results

It can be seen from the calculation results as given in Fig. 3 that the separation efficiency error between experiment result and simulation computation result doesn't exceed 2%. It means that the calculation result of the simulation model established is reliable, and it can be used to simulate calculation on the separation efficiency of the Enclosed Sand Separator designed.

ONE-STAGE SEPARATION TANK OPTIMIZATION

When the dimension of the tank body has been determined, main factors that will pose influence on the separation efficiency and service life of the one-stage separation tank: inlet position (as shown in Fig. 3), distance of sand removal baffle (dimension c in Fig. 2) and height of sand removal baffle from the dedusting liquid surface (dimension d in Fig.2). The one-stage separation tank is optimized herein with such objectives as low peak pressure inside the separation tank and less content of solid in the outlet.

In order to better judge the superiority of schemes, this thesis defines the product of maximum pressure inside the tank and solid flow rate in the outlet as PMM, where P_{max} maximum pressure inside the tank (kPa), Q mass flow of solid in the outlet (kg/min):

$$\text{PMM} = P_{max} \times Q \tag{13}$$

Mass flow of solid in the outlet and maximum pressure inside the tank under the condition of different schemes will be calculated by using the gas liquid solid three phase computational fluid dynamics model in section 3.

When the pressure within the tank is within the construction safety scope, smaller PMM means more reasonableness of the scheme.

Inlet schemes contrast

Keep the length of pipeline in the inlet on both sides consistent, and assume the distance from the middle inlet to the tank interior wall in the inlet side a, and distance from inlet on both sides to the tank interior wall in the inlet side b. Compare four inlet position schemes, respectively: a=b=1100mm; a=b=2500mm; a=1100mm, b=2500mm; a=2500mm, b=1100mm. The structure schematics is given in Fig.4.

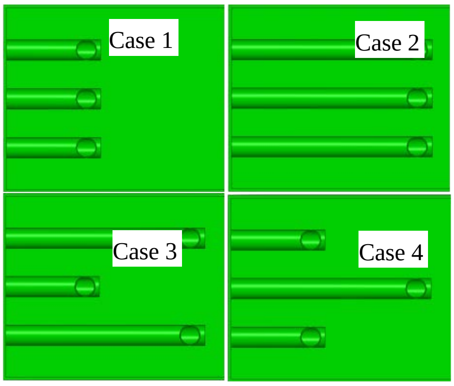

Fig.4 A bird's view of inlet position of four schemes

Pressure cloud chart (relative pressure) of four inlet schemes in the middle cross section is given in Figure 5:

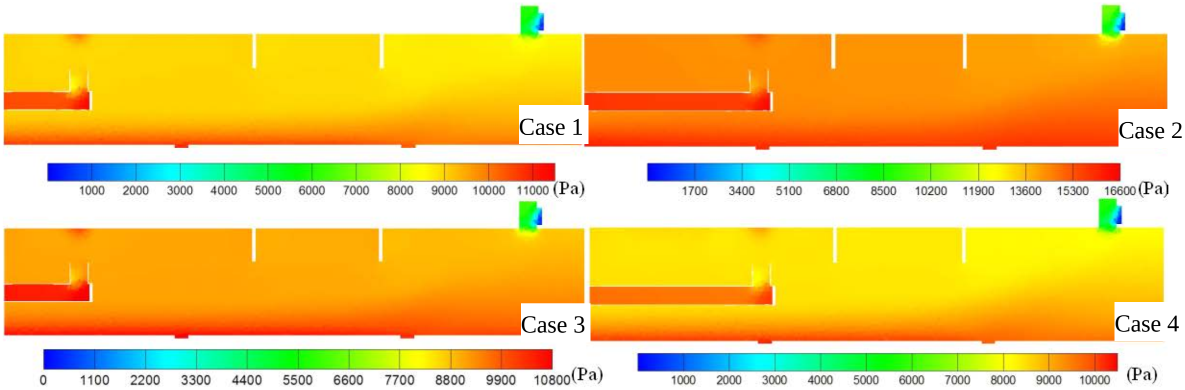

Fig.5 Pressure cloud chart of four schemes in the middle cross section

Table 1 Outlet solid mass flow and maximum pressure inside the tank with respect to four schemes

Scheme	*Outlet solid mass flow（kg/min）*	*Maximum pressure inside tank（kPa）*
Scheme 1	9.66	11. 3
Scheme 2	11.16	16 .6
Scheme 3	9.31	10 .8
Scheme 4	10.26	12 .4

It can be seen from the pressure cloud chart as given in Fig.5: positions of maximum pressure inside the one-stage separation tank are mainly concentrated on the inlet pipeline; the inlet pipeline and gas drilling sand drainage pipeline are connected; therefore, when the pressure inside the inlet pipeline is smaller, gas and sand inside the sand drainage pipeline easily discharge. Conversely, when the pressure inside the inlet pipeline is too big, it will hamper the discharge of gas flow and the rock carrying effect, or even affect the normal proceeding of the gas drilling. It can be known based on table 1: scheme 3 with shorter middle inlet pipeline, and longer inlet pipeline on both ends boasts of minimum pressure inside the pipeline. Besides, the solid content in the outlet is lowest (namely the dust removal efficiency is highest); therefore, the one stage separation tank inlet structure as given in scheme 3 can be used to reduce pressure inside the tank and improve the separation efficiency.

Optimization of length of inlet in the middle (dimension a)

As shown in Fig.6, with respect to the multiple length schemes of dimension a with b=2500mm, it can be seen from the trendline chart of the solid mass flow in the outlet, maximum pressure inside the tank and PMM: in case of a=800mm, pressure inside the tank is lower, and the solid mass flow in the outlet is minimum, and PMM is lowest. Therefore, when using the scheme of a=800mm, the return pressure in the wellhead sand drainage pipeline is small, and the dust removal effect is good. In case of a ＞1900mm, pressure inside the tank and solid content in the outlet rapidly increase. Therefore, it's strictly prohibited during design that the middle inlet length is more than 1900mm.

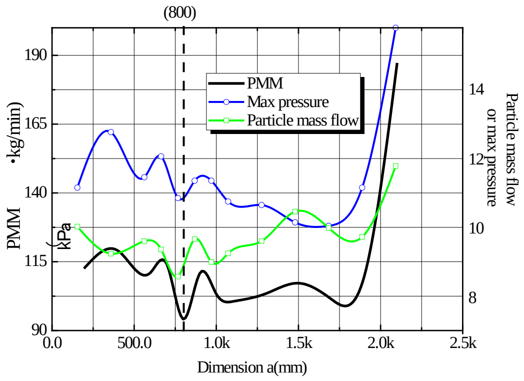

Fig.6 Particle mass flow, max pressure and PMM at different length of a

Optimization of length of inlet on both sides (dimension b)

As shown in Fig.7, with respect to the multiple length schemes of dimension b, it can be seen from the trendline chart of the solid mass flow in the outlet, maximum pressure inside the tank and PMM: in case of a=800mm, in case of b＜2100mm, peak pressure inside the tank, solid content in the outlet and PMM are all higher; in case of b＞2700mm, items abovementioned are on the rise; in case of length of inlet on both sides 2500mm, maximum pressure inside the tank is lower, which won't form pressure out in the sand drainage pipeline; besides, the solid mass flow in the outlet is small, and PMM is lowest. Therefore, during design, the length of inlet on both sides shall be controlled within 2100mm~2700mm. This thesis thus adopts the inlet scheme of a=800mm, b=2500mm.

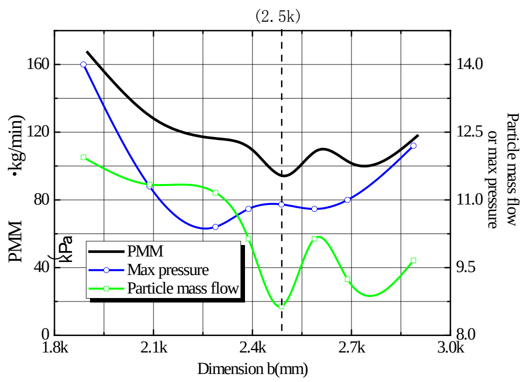

Fig.7 Particle mass flow, max pressure and PMM at different length of b

Optimization of dedusting baffle distance (dimension c)

As shown in Fig.8, with respect to the aforementioned inlet schemes, it can be seen from the trendline chart of the solid mass flow in the outlet, maximum pressure inside the tank and PMM under multiple lengths of dimension c: during the process when c increases from 1600mm to 2900mm, maximum value of pressure inside the tank gradually reduces; in case of c＞2900mm, pressure inside the tank rapidly increases; therefore, c shall be within the scope of being slightly lower than 2900mm; the solid flow in the outlet is constantly on fluctuation, which is because that the space and position of gas flow blocked by the baffle is different since distances from three inlets to the sand removal baffle are inconsistent; during c=2600mm, PMM is optimum, and the peak value inside the tank is lower. Therefore, the scheme of c=2600mm is adopted.

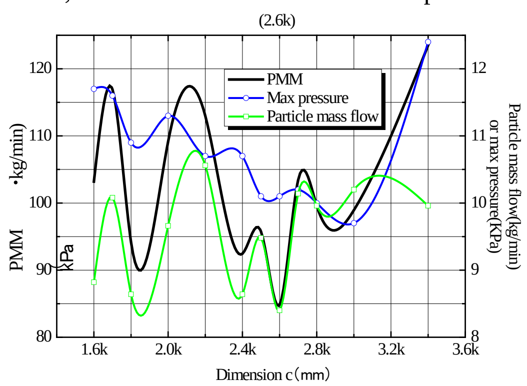

Fig.8 Particle mass flow, max pressure and PMM at different length of c

Optimization of distance from the bottom of sand removal baffle to dedusting liquid surface (dimension d)

As shown in Fig.2, one-stage separation tank reserves 900mm-deep dedusting liquid; assume that the dedusting liquid surface remains unchanged, optimize the distance from the baffle bottom to the dedusting liquid surface by changing the baffle height. Calculate the influence on the content of solid in the outlet and maximum pressure inside the tank.

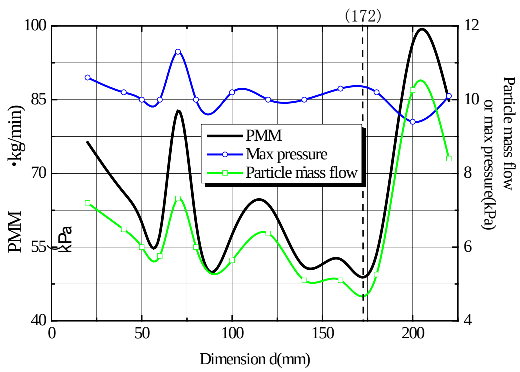

Fig.9 Particle mass flow, max pressure and PMM at different length of d

As shown in Fig.9, it can be seen from the trendline chart of the solid mass flow in the outlet, maximum pressure inside the tank and PMM: in case of 80mm＜d＜220mm, fluctuation of peak pressure inside the tank is lower, and the lower pressure level sustains; when the d value further decreases, peak pressure inside the tank has the trend of increase, and the over small distance leads to reduction of dedusting efficiency; in case of 80mm＜d＜180mm, the dedusting effect is good, and PMM is lower; therefore, the distance from the baffle bottom to the dedusting liquid surface shall be within such scope. In case of d=172mm, PMM is lowest. Therefore, such scheme is adopted herein.

It can be seen from the particle motion trajectory as shown in Fig.10, the gas flow gushes out upward; the gas flow gushing out from the inlet impacts the roof and spreads out; some gas flow after obstruction enters the dedusting liquid, and most gas flow moves towards the outlet; some gas flow after obstruction will again enter the dedusting fluid, and the majority of gas flow moves towards the outlet. After obstruction by the 1st baffle, the gas flow moves downward, and it again forces some gas flow to enter the dedusting fluid; after obstruction by the 1st baffle, the gas flow moves towards the roof plate, and the vortex is formed after the 1st baffle; when the gas flow moves to the roof plate and is blocked by the 2nd baffle, some gas flow again enters the dedusting fluid; the gas flow out of the clearance between the baffle bottom and the dedusting fluid surface will form vortex behind the 2nd baffle and enter the two stage separation tank via the outlet. The stop effect of roof plate, change of gas flow motion direction by the 1st and 2nd baffle and vortex behind the baffle help improve the dedusting effect of the one stage separation tank.

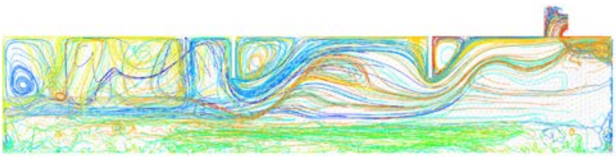

Fig.10 One stage separation tank particle motion trajectory

TWO STAGE SEPARATION TANK DUST REMOVAL EFFICIENCY CALCULATION AND SAND REMOVAL BAFFLE SCHEME OPTIMIZATION

In the two stage separation tank, reasonable tapping layout of dedusting baffle can stop powder dust that has been removed by the dedusting liquid; by changing the motion direction of the powder dust, it may again enter the dedusting liquid so as to improve the separation efficiency. Therefore, in this section, the submerged sieve pipe and hole scheme and sand removal baffle scheme will be optimized to secure sand removal efficiency and operation safety. Therefore, the dust removal efficiency and allocation of the phase volume fraction may be calculated under conditions of no baffle, distance from single-layer baffle to dedusting liquid surface 430mm and distance from single-layer baffle to dedusting liquid surface 100mm and double-layer baffle.

It can be seen in Fig.11: when the baffle tapping diameter is 100mm, with respect to the volume fraction of dedusting liquid inside the two stage separation tank under four baffle schemes; when there is no baffle, the rising height of dedusting liquid is slightly higher; however, the liquid surface near the outlet is relatively steady; when the distance from the baffle to the dedusting liquid is 430mm, the baffle in the inlet end blocks some upward moving dedusting fluid; besides, it may further block the wet gas flow via the water batch dedusting, and improve the dedusting efficiency; when the distance from the baffle to the dedusting liquid surface is 100mm, the baffle obviously blocks the upward surging of the dedusting liquid, and plentiful dedusting liquid overflows via the baffle hole. Besides, smaller baffle holes increase the upward movement speed of the dedusting liquid so that it may easily lead to such safety incidents as gushing out of the dedusting fluid via the outlet or the outlet plugging; with respect to the double-layer baffle, two-layer baffle holes are alternatively placed so that the upper baffle effectively blocks the dedusting fluid flowing out of holes in the lower baffle, and the motion direction of wet gas flow changes. Parallel with securing that the dedusting fluid doesn't gush out, the reasonable layout of double-layer baffle can further improve the dedusting efficiency.

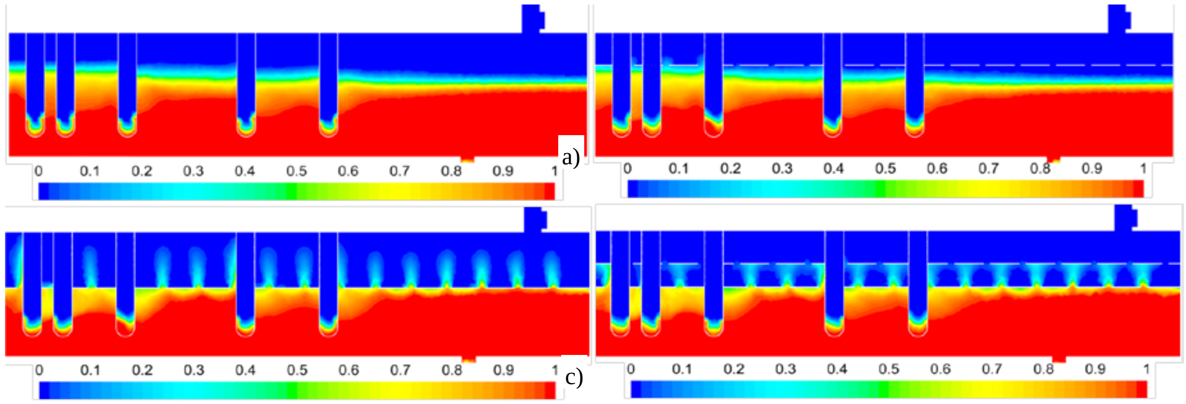

Fig.11 Two stage separation tank middle cross section dedusting liquid volume fraction (a no baffle; b distance from single-layer baffle to dedusting liquid surface 430mm; c distance from single-layer baffle to dedusting liquid surface 100mm; d double-layer baffle)

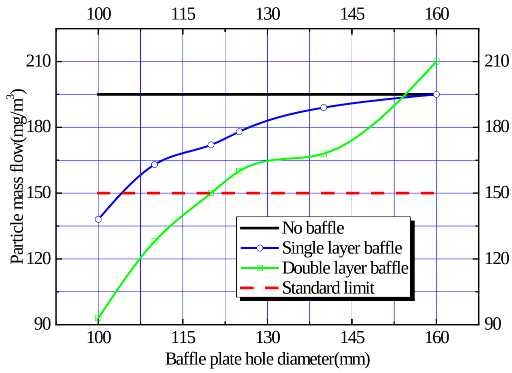

Fig.12 Solid content in outlet (distance from single-layer baffle to dedusting liquid surface 430mm)

It can be seen from the solid content with respect to different plans as shown in Fig.12, the solid content in the outlet without baffle is higher; solid content in the outlet for the single-layer baffle and double-layer baffle increases with the increase of the diameter of the baffle hole; due to the hole diameter and match of the double-layer baffle, when the baffle hole diameter reaches a certain extent, the solid content in the outlet is even higher than that without baffle. It can be seen from the figure: when there is no baffle, the solid content in the outlet cannot reach the emission standard of air pollutant; under the condition of single-layer baffle, the standard limit can only be reached when the hole diameter is less than 104mm; under the condition of double-layer baffle, the standard limit as provided by GB16297-1996 may only be reached when the hole diameter is less than 119mm.

FIELD APPLICATION

Based on the aforesaid dimension after structural optimization, the Enclosed Sand Separator for the gas drilling designed is produced and applied to the gas drilling of YangJia 1st well (as shown in Fig.13). Such device effectively removes sand from the gas drilling, and protects the well pad operation environment. The gas recycling can be realized when the outlet of the two stage separation tank is connected with the gas compressor.

Fig.13 Test of the Enclosed Sand Separator in YangJia 1st well.

CONCLUSIONS

Because environment pollution during gas drilling is serious, and the recycling gas drilling cannot be implemented because of lack of reasonable sand removal equipment, this thesis draws conclusions below with respect to the design of the Enclosed Sand Separator and based on the gas liquid solid three phase flow field analysis:

1）The Enclosed Sand Separator composing of two stages has been designed, and sand contained in the gas flow is split via the gravity, inertia and water bath separation.

2）Split the gas liquid solid three phase into the quasi three phase flow of mixture of gas liquid and gas solid; simulate gas phase via the standard k-ε model and simulate gas liquid and gas solid via Eular multiphase flow model, establish the gas liquid solid three phase flow model for the simulation of flow field inside the Enclosed Sand Separator designed, and validate the correctness of the model calculation results through contrast and experiment.

3）Based on the gas liquid solid three phase flow model for the Enclosed Sand Separator established, and optimize the inlet scheme, middle inlet length a, length of inlet on both sides b, sand removal baffle distance c and distance from the sand removal baffle bottom to the dedusting liquid surface d by taking small PMM as the evaluation standard, and the good structure is obtained.

4）The Enclosed Sand Separator for gas drilling designed herein is successfully applied to YangJia 1st well, and the gas flow after separation can meet with GB16297-1996.

ACKNOWLEDGEMENT

This research is supported by Open Fund(OGE201702-27) of Key Laboratory of Oil &Gas Equipment，Ministry of Education (Southwest Petroleum University), Scientific Research Starting Project of SWPU (No. 2017QHZ012), Major Project by Education Office of Sichuan Province (No. 17ZA0418), the Natural Science Fund (Grant No. 51674214), Youth Scientific Research Innovation Team Project of Sichuan Province (2017TD0014), International Cooperation Project of Sichuan Science and Technology plan (2016HH0008）.

REFERENCES

Fu Jianhong, Song Kexiong, Zhang Zhi, et al. Stress Analysis on Drilling String Vibration in Gas Drilling[J]. Energy Procedia, 2012, 16:1264-1268.

Committee ASME Shale Shaker. Drilling Fluids Processing Handbook[M]. America Gulf Professional Publishing, 2005.

John H. Hallman Muhammad A. Muqeem Clark. Fluid Customization and Equipment Optimization Enable Safe and Successful Underbalanced Drilling of High-H2S Horizonttal Wells in Saudi Arabia: IADS/SPE Managed Pressure Drilling and Underbalanced Operations Conference and Exhibiton, 2007[C].

Muhammad A. Muqeem Clark M. Jarrett Hassan. Underbalanced Drilling of Oil Wells in Saudi Arabia: Case History and Lessons Learned: IADC/SPE Managed Pressure Drilling and Underbalanced Operations Conference and Exhibiton, 2008[C].

Croom M. L. Effective Selection of Filter Dust Collectors[J]. Chemical Engineering, 1993, 100(7):86-91.

Agarwal A. Design Guide for Dust Collectors[J]. Chemical Engineering, 2005, 112(2):42-49.

Shannon M. J. Understanding and Selecting Dust Collectors[J]. Journal of Protective Coatings & Linings, 1996, 13(5):37-42.

Cagna M. Boehle M. Application of CFD methods for the simulation of the flow through a filter in dependency of the operating time[J]. Fluids Engineering Division, 2002, 257(1):1013-1017.

Abrahamson John, Jones Roger, Lau Andy, et al. Influence of entry duct bends on the performance of return-flow cyclone dust collectors[J]. Powder Technology, 2002, 123(2－3):126-137.

Avci Atakan, Karagoz Irfan, Surmen Ali. Development of a new method for evaluating vortex length in reversed flow cyclone separators[J]. Powder Technology, 2013, 235(2):460-466.

Tian C, YJ. Lu. Turbulence model models of separated flow in shock wave thrust vector nozzle[J]. Engineering Applications of Computational Fluid Mechanics, 2013, 7:182-192.

Li Shan-hong Li Cai-ting Zeng Guang-ming. CFD simulation on performance of new type umbrella plate scrubber[J]. Transactions of Nonferrous Metals Society of China, 2008, 18(02):488-492.

Tanthapanichakoon W., Charinpanitkul T., Jintaworn W., et al. CFD investigation of high-temperature gas filtration using twin ceramic candles[J]. Powder Technology, 2008, 180(1－2):245-252.

Chu K. W., Wang B., Xu D. L., et al. CFD–DEM simulation of the gas–solid flow in a cyclone separator[J]. Chemical Engineering Science, 2011, 66(5):834-847.

Manju M. S., Savithri S. Three dimensional CFD simulation of pneumatic coal injection in a direct reduction rotary kiln[J]. Fuel, 2012, 102:54-64.

Lopes Rodrigo J. G., Quinta-Ferreira Rosa M. CFD modelling of multiphase flow distribution in trickle beds[J]. CHEMICAL ENGINEERING JOURNAL, 2009, 147(2-3):342-355.

Marocco Luca, Inzoli Fabio. Multiphase Euler–Lagrange CFD simulation applied to Wet Flue Gas Desulphurisation technology[J]. International Journal of Multiphase Flow, 2009, 35(2):185-194.

X. Romaní, Fernández X. R., Nirschl H. Multiphase CFD Simulation of a Solid Bowl Centrifuge[J]. Chemical Engineering & Technology, 2009, 32(5):719-725.

Shukla S. K., Shukla P., Ghosh P. Evaluation of Numerical Schemes for Dispersed Phase Modeling of Cyclone Separators[J]. Engineering Applications of Computational Flui..., 2011.

Jung Chang H., Kim Yong P. Analysis on the bias of the PM2.5 separator for polydispersed aerosol size distribution[J]. Separation and Purification Technology, 2013, 104:167-174.

Eslamian Morteza, Saghir M. Ziad. Novel thermophoretic particle separators: Numerical analysis and simulation[J]. Applied Thermal Engineering, 2013, 59(1–2):527-534.

Gao Xiang, Chen Jinfeng, Feng Jianmei, et al. Numerical and experimental investigations of the?effects of the breakup of oil droplets on the performance of oil–gas cyclone separators in oil-injected compressor systems[J]. International Journal of Refrigeration, 2013, 36(7):1894-1904.

Hreiz Rainier, Lainé Richard, Wu Jing, et al. On the effect of the nozzle design on the performances of gas–liquid cylindrical cyclone separators[J]. International Journal of Multiphase Flow, 2014, 58:15-26.

Xiong Zhiyi, Ji Zhongli, Wu Xiaolin. Development of a cyclone separator with high efficiency and low pressure drop in axial inlet cyclones[J]. Powder Technology, 2014, 253:644-649.

Xiong Zhenqin, Lu Mingchao, Wang Minglu, et al. Study on flow pattern and separation performance of air–water swirl-vane separator[J]. Annals of Nuclear Energy, 2014, 63:138-145.

Karagoz Irfan, Avci Atakan, Surmen Ali, et al. Design and performance evaluation of a new cyclone separator[J]. Journal of Aerosol Science, 2013, 59:57-64.

Arvoh Benjamin Kaku, Skeie Nils-Olav, Halstensen Maths. Estimation of gas/liquid and oil/water interface levels in an oil/water/gas separator based on pressure measurements and regression modelling[J]. Separation and Purification Technology, 2013, 107:204-210.

Khan Zoheb, Joshi Jyeshtharaj B. Comparison of k–ε, RSM and LES models for the prediction of flow pattern in jet loop reactor[J]. Chemical Engineering Science, 2015, 127:323-333.

NOMENCLATURE

ρ : media concentration

k : turbulence energy

u_i : fluid velocity of phase i direction

$C_{1\varepsilon}$, $C_{2\varepsilon}$, $C_{3\varepsilon}$: empirical constant

σ_k : Prandtl number corresponding to turbulence energy k

σ_ε : Prandtl number corresponding to dissipation rate ε

ε : dissipation rate of turbulence energy

μ_t : turbulence viscosity

G_k : average velocity gradient

G_b : buoyance

$\Pr_t$: Prandtl number of turbulence energy

g_i : component of acceleration of gravity in i direction

α : coefficient of thermal expansion

Y_M : contribution of pulse expansion to the compressible turbulence

a : acoustic velocity

subscript p : phase

subscript g : gas phase

subscript l : liquid phase

subscript s : solid phase

φ : phase volume fraction

superscript f : pulse momentum

F_p : interphase force

E_p : viscous stress

$\overline{F_p}$: drag force between gas solid phase

β : function of drag force between two phases

PMM: product of maximum pressure inside the tank and solid flow rate in the outlet

$P_{\max}$: maximum pressure inside the tank

Q : mass flow of solid in the outlet